C2012-0001752

NACE INTERNATIONAL CORROSION 2012 CONFERENCE & EXPO

Corrosion of Steel in Cracked Reinforced Concrete Pipes

Ezeddin Busba and Alberto A. Sagüés
Dept. of Civil and Environmental Engineering, University of South Florida
4202 E. Fowler Ave. ENB118
Tampa, FL 33620

ABSTRACT

Reinforced concrete pipes are commonly used for culvert and storm drainage applications and are intended to last for several decades. The effect of cracks on corrosion of embedded reinforcing ~3/16 in (~4.75 mm) diameter steel wires was investigated. Cracks having a nominal width of 0.02 and 0.1 inch (~ 0.5 and ~2.5 mm) were induced by 3-point bending on the interior surface of quadrants extracted from 18inch (45 cm)-diameter concrete pipes. Two types of concrete pipes were examined and referred to as Z-type and R-type with average interior concrete covers of 1.2 and 0.7 inch (30.5 and ~17.8 mm) respectively. The Z-type contained higher cement content whereas the R-type had a 20 % fly ash replacement. The cracked specimens along with controls were tested under both continuous and 1 week-dry/1 week-wet cyclic exposures to 500 ppm chloride solution for periods of 115 days and 7 cycles respectively. Open circuit potential and electrochemical impedance measurements were performed. Electrochemical test results were calibrated using data obtained from destructive examination of wire corrosion. Data analysis showed that corrosion current increased as the crack width-to-cover ratio increased for both types. Corrosion-based projection models indicated strongly enhanced performance for the 0.02-inch (~0.5 mm) cases compared to the 0.1-inch (~2.5 mm) cases.

Key words: Reinforced concrete pipe, crack, corrosion, durability.

INTRODUCTION

Reinforced concrete pipes (RCP) are widely used in installations requiring service over a period of many decades, so only extremely slow deterioration with time can be accepted. Concrete cracks are often revealed by inspections conducted on recently placed pipes. In-place RCP cracks can degrade pipe performance by decreasing structural strength and dimensional stability, permitting leaks and marginally increasing hydraulic resistance, and by allowing premature corrosion of steel reinforcement.[1-3] At the bottom of such cracks bare steel is likely to be directly exposed to water which, if renewed regularly by flow, would eventually have a pH close to that of the environment. Under neutral and mildly acidic conditions and with natural aeration the steel surface is active, and corrodes where exposed. Galvanic coupling with nearby cathodic steel embedded in the concrete could dramatically aggravate local corrosion of the steel, leading to quick section loss and mechanical failure if under tension.[4] Of possibly greater concern than wire failure is the earlier development of expansive corrosion products at the crack location and nearby influence zone, because of resulting concrete spalls with potentially severe increase in hydraulic resistance and obstructions as well as loss of load bearing wall thickness. Mitigating factors exist, especially autogenous healing (AH) that can assist in closing concrete cracks by precipitation of compounds such as calcium carbonate.[5] AH is more prevalent with thinner cracks, with a recent review of the literature indicating that there was a reasonable expectation for AH to eventually occur in RCP for highway drainage applications when preexisting cracks were narrower than about 0.020 in (0.5 mm), with increasingly less favorably prognosis as wider cracks were considered.[6] Existing guidelines for acceptability of in-place RCP cracking reflect those observations to some extent.[7] The AH process nevertheless may take a few years to fully develop, so there is interest in determining to which extent corrosion of the reinforcing wires may occur in the interim. This investigation addressed that issue by corrosion tests and modeling for commercial production RCP with controlled amounts of cracking.

EXPERIMENTAL PROCEDURE

Materials and Specimen Preparation

RC pipes from two different pipe manufacturing sources were evaluated for the possible extent of reinforcement corrosion at preexisting cracks in a moderately aggressive simulated natural water environment. The pipes 8 ft (2.4 m) long X 18 inch (45 cm) in diameter were manufactured in accordance with ASTM C76, and designated by the code names R-Type and Z-Type.[8] Both types were class III B-wall having 2.5 in (63.5 mm) wall thickness, 1 in (25.4 mm) nominal interior concrete cover and a reinforcing steel wire diameter (D) ~3/16 in (4.75mm). Product materials are listed in Table 1. The R-Type concrete mix contains fly ash whereas that of Z-Type has not but includes higher cement content.

Table 1
Mixture proportions of the R-Type and Z-Type pipes as reported by manufacturers

Mix design 4000 PSI			
Material Type	Material Quantity		Unit
	R	Z	
Cement	391 (232)	590 (350)	lb/yd^3 (kg/m^3)
Fly ash	103 (61)	0	lb/yd^3 (kg/m^3)
sand	1689 (1001)	1895 (1124)	lb/yd^3 (kg/m^3)
stone	1773 (1051)	1300 (771)	lb/yd^3 (kg/m^3)
water	16 (79)	29 (143)	gal/yd^3 (Lit/m^3)
Admixture	0	0	oz

Figure 1 illustrates how an RC pipe was sectioned into two pipe rings that were in turn cut into quadrants to produce 8 test specimens. Two pipes from each type produced a total of 32 specimens.

For all the as-cut specimens, measurement of the interior concrete cover thickness was made by direct ruler readings on the four cut edges at all exposed reinforcing wires. Statistical analysis of data for pipe sections from each manufacturer indicated that Z-type specimens have a thicker internal cover ranging from 0.6 in to 1.75 in (15.25 mm to 44.45 mm) than R-type specimens ranging from 0.4 in to 1.1 in (10 mm to 28 mm) .Table 2 shows the average concrete cover values for the test specimens.

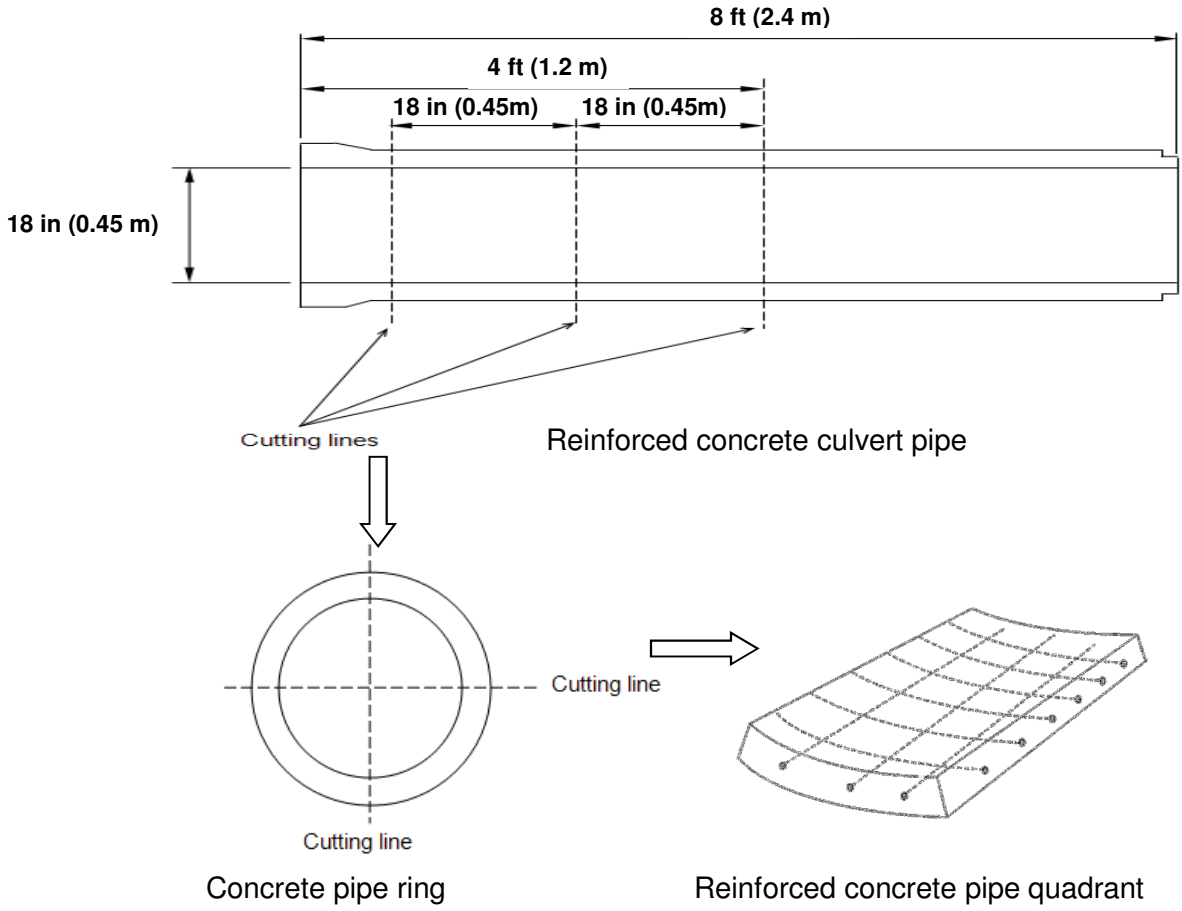

Figure 1: RCP sectioned to produce 8 quadrants

Importantly, cross sections of the pipe wall exposed during cutting revealed that the reinforcement of the Z-type pipes had extensive consolidation voids around the circumferential wires apparently due to unconsolidated concrete, Figure 2. The voids seemed to be forming a tunnel running along the entire length of wires.

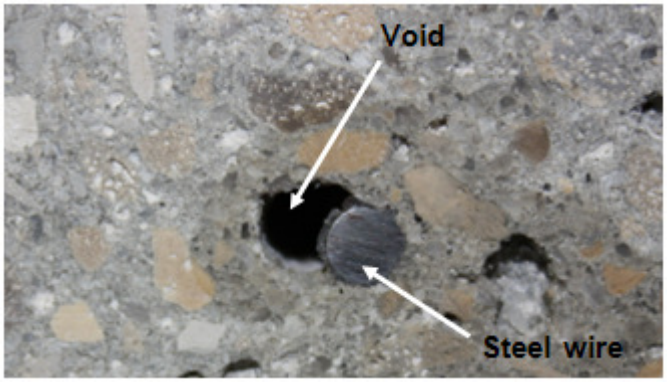

Figure 2: A magnified image of a Z-type specimen showing consolidation void next to circumferential steel wire at the cutting edge

For the evaluations, specimens cut out of the pipes were cracked to obtain target; narrow (0.02 in) and wide (0.1 in) openings, representing a case with recognized potential for future AH and one with much poorer prognosis respectively. [6, 7] Uncracked specimens served as controls. The cracks were intended to be single with a total length of 18 in (45 cm) and extending lengthwise parallel to the direction from the bell side to the spigot side of a pipe. Figure 3a shows the cracking rig applying 3-point loading to induce the cracks. The crack width was monitored during loading. After cracking was completed, more detailed measurements of crack width, Figure 3b, and depth were performed using a crack comparator and insertion gauges at ½ in (~ 12.5 mm) intervals along the entire length of a crack. Table 2 shows the achieved crack width and depth values as well as the average measured interior concrete cover. All specimens having a 0.02 inch (~0.5 mm) crack width are referred to herein after in the text and figures as 0.02 in- crack class. Likewise all specimens having a 0.1 inch (~2.5 mm) crack width are referred to as 0.1 in-crack class.

Plexiglas exposure ponds, with footprint area 9 in x 14 in (23 cm x 35.5 cm) sealed with silicone sealant, were used. Both crack ends as well as the area at the back side of the specimen facing the crack were also sealed with epoxy to prevent leak through the crack.

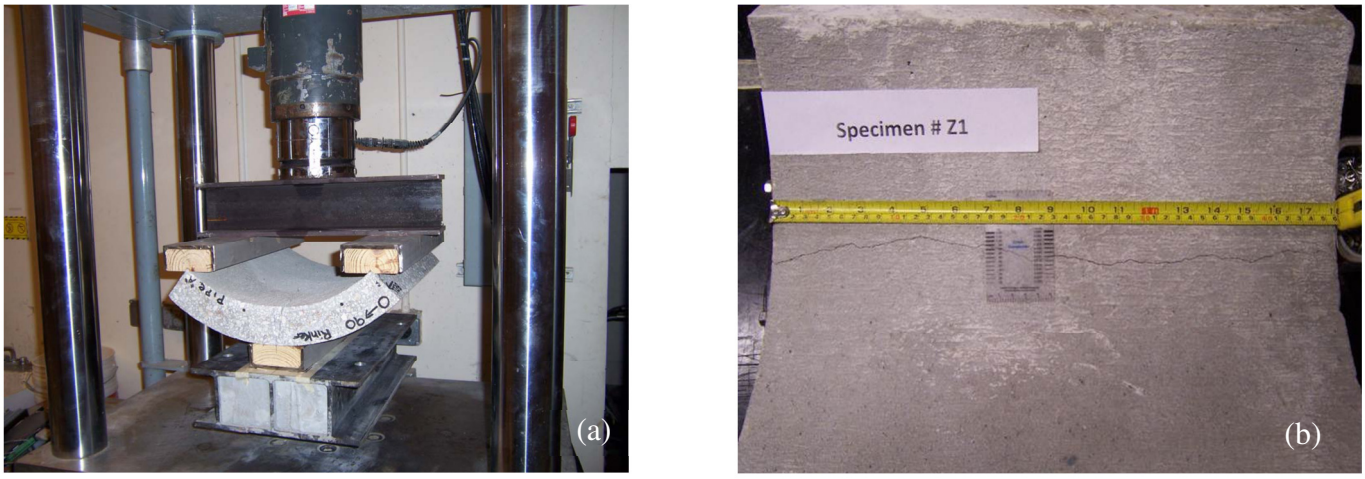

Figure 3: (a) Cracking rig used to generate cracks in RC culvert pipe specimens, (b) Top view for 0.01 in (~2.5 mm) Z-type specimen showing Crack width measurement along a crack using a crack comparator.

Table 2
Crack width and depth data for R- and Z-type specimens

Type	Specimen #	Target crack width / in (mm)	Average internal cover / in (mm)	Achieved crack Width / in (mm)		Average achieved crack depth / in (mm)	Average crack depth intersecting wire	Maximum crack depth intersecting wire	Remark
				Average	Standard deviation				
R	R7	0	0.846 (21.48)	-	-	-	-	-	Control
	R10		0.675 (17.14)	-	-	-	-	-	Control
	R3	0.020 (0.5)	0.734 (18.64)	0.028 (0.711)	0.006 (0.152)	0.331 (8.407)			
	R6		0.796 (20.21)	0.018 (0.457)	0.003 (0.076)	0.254 (6.451)			
	R12	0.100 (2.5)	0.741 (18.82)	0.106 (2.69)	0.049 (1.244)	1.288 (32.715)	Yes	Yes	
	R4		0.936 (23.77)	0.067 (1.70)	0.015 (0.381)	1.124 (28.549)	Yes	Yes	
Z	Z6	0	1.282 (32.56)	-	-	-	-	-	Control
	ZB		1.253 (31.82)	-	-	-	-	-	Control
	Z1	0.020 (0.5)	1.308 (33.22)	0.017 (0.431)	0.004 (0.101)	0.196 (4.978)			
	Z13		1.315 (33.40)	0.021 (0.533)	0.006 (0.152)	0.208 (5.283)			
	Z11	0.100 (2.5)	1.045 (26.54)	0.116 (2.94)	0.042 (1.066)	1.343 (34.112)	Yes	Yes	
	Z14		1.126 (28.60)	0.093 (2.36)	0.019 (0.482)	1.18 (29.972)	Yes	Yes	

Environmental Exposure

The cracked and uncracked specimens from both the R- and Z-type specimens, (shown in Table 2), were tested for corrosion resistance. All exposures were conducted at lab temperature of ~ 25°C.The specimens were first subjected to continuous ponding with de-ionized (DI) water for 33 days. This prior exposure to DI water was conducted to allow the specimen steel potentials to reach a steady state condition in a slightly aggressive environment, thus allowing for further insight on the effect of introducing the more aggressive medium for the main portions of the test. After 33 days the ponding medium was changed to distilled water with the addition of sodium chloride to obtain a 500 ppm chloride ion concentration for a period of 115 days. The solution as prepared was near neutral but pH in the pond stabilized to a value of ~ 8.7 after a period of 1 month. Following continuous exposure to the chloride containing environment, the specimens were exposed to 7 cycles of 1 week dry / 1 week wet cyclic ponding using the same test medium as that of the continuous ponding regime. During the cyclic exposure, a newly prepared solution was used for each wet cycle. The cycling was adopted to highlight the importance of evaporative chloride concentration in creating highly corrosive environment.
The test cycle was accelerated to evaluate the extent of corrosion damage that a mild chloride environment can cause to a cracked RCP in the absence of any mitigating factors (e.g. AH). However, RCP may not be exposed to severe cycling frequency in service.

Electrochemical Assessment

Reinforcing steel potentials were measured regularly before and during exposure to chloride. All potential measurements were made using a saturated calomel reference electrode (SCE) placed at the center of the pond with its tip immersed in water. Potential mapping were also performed at 1 in by 1 in

grid traced on the inner surface of the pond footprint. Electrochemical Impedance Spectroscopy (EIS) testing was performed to determine the corrosion current of embedded reinforcing steel before and after exposure to the chloride containing solution. The frequency range evaluated had an upper end of 1000 Hz. The lower end was 10 mHz (during the chloride-free exposure period) or 3 mHz (after chloride addition) for additional fast measurements that could be conducted easily, and 1 mHz for slower experiments designed to better sample the lower frequency range which typically contains much of the information relevant to corrosion rate determination. Excitation amplitude was 10 mV. The reference electrode used was the SCE placed in the solution same as in the potential measurements. The counter electrode was an activated titanium mesh immersed in solution and covering the entire pond footprint.

The equivalent circuit, used for simplified interpretation of the electrochemical impedance data, consists of a solution resistance Rs connected in series with a parallel combination of a polarization resistance component Rp, associated with the corrosion process, with a constant phase angle element (CPE) component representing an interfacial charge storage process.[9] The CPE has impedance Z_{CPE} given by:

$$Z_{CPE} = 1/ [Y_o (j \omega)^n] \quad (1)$$

Where; Y_o is a constant and n is a real number between 0 and 1; $j = (-1)^{1/2}$ and, $\omega = 2 \pi f$ (where f is frequency).

The equivalent circuit total impedance Z_T is given by:

$$Z_T = R_s + \{ 1 / [Y_o (j \omega)^n + R_p^{-1}] \} \quad (2)$$

The impedance parameters Rs, R_p, Y_o and n were determined by fitting the measured total impedance data over a selected frequency range with the equivalent circuit total impedance values over the same range. The analyzed frequency range was selected to include the data from 10 mHz and lower.

The nominal corrosion current (I_{corr}) was estimated by:

$$I_{corr} = B / Rp \quad (3)$$

where B is Stern-Geary coefficient and is approximated as 26 mV for corroding steel in concrete.[9, 10] A calibration factor was applied afterwards as detailed next.

Direct Corrosion Assessment

Visual appearance of the crack zone was monitored regularly for evidence of rust formation. At the end of the present exposure schedule one specimen of the 0.02 and 0.1-in (0.5 and 2.5-mm)-wide crack classes was broken open from each type of RCP (specimens R6, R12, Z1 and Z11). The remaining specimens are to be autopsied in follow up testing. The extent of the corrosion influence zone was examined and the amount of radius loss was measured using a digital caliper and the data supplemented by analysis of close-up wire images. For each specimen autopsied the total amount of actual mass loss was calculated and compared with the nominal total mass loss estimated from the integrated I_{corr} data for the same specimen. A calibration factor was derived for each class and then applied to the EIS results for all specimens of the same class. The resulting corrected values were used for the corrosion damage projection forecast.

RESULTS AND DISCUSSION

Both direct observations and electrochemical testing provided evidence of significant corrosion in progress, especially at the wider crack locations. That evidence supported the concern stated in the Introduction that steel exposed at the bottom of relatively large cracks faces a solution that is much less alkaline than the pore water of the concrete. That condition is likely the result of efficient diffusional and convective mixing inside the wide crack between any leachates from the concrete pore waters at the crack walls, and the exterior water. The resulting lowered electrolyte pH is less supportive of a stable passive regime and breakdown may occur even at very low chloride contents.

Some of the Z- and R-type specimens having 0.1-in-wide cracks (Z11 and R12) exhibited external visual signs of rust as early as about one week after chloride exposure began. Figure 4 shows the corrosion product evolution of specimen Z11 during the continuous chloride exposure period at one of the intersections of the circumferential steel wires with the crack. Specimen R4 showed a corrosion spot at the steel wire-crack intersection close to the edge after 52 days. There was no external corrosion product observed in specimen Z14, nor in the specimens having 0.02-in-wide cracks (R3, R6, Z1 and Z13).

Open circuit potential (OCP) served as a supplemental indicator of corrosion condition.[9] As detailed in ASTM C-876, highly negative potentials in atmospherically exposed concrete are symptomatic of ongoing active corrosion of concrete reinforcement, while less negative values are associated with passive, low corrosion rate conditions.[11] Figure 5 shows the open circuit potential values averaged over each of the three exposure periods and for each pair of replicate test specimens. Replicate specimens yielded potential values comparable to each other. The control (uncracked) specimens of both types showed, as expected, less negative OCP values typical of those expected for passive steel in concrete. In contrast, the 0.1-in-width crack specimens showed highly negative potentials, even in the chloride-free initial exposure phase.

The OCP values for the 0.02-in-crack width-specimens were distinctly more negative than those of the uncracked controls, strongly indicating some extent of active corrosion as well even with the narrow cracks. The conditions responsible for activation are expected to be similar to that for the wider cracks. Some mitigation existed as the OCP values were not as negative as those for the wider crack specimens, likely indicating that activation at the bottom of the narrower cracks happened at fewer crack-steel wire intersection points, or that the size or the corrosion zones was smaller. Importantly, the OCP indications of corrosion were present regardless of the differences between the concrete compositions used by the suppliers.

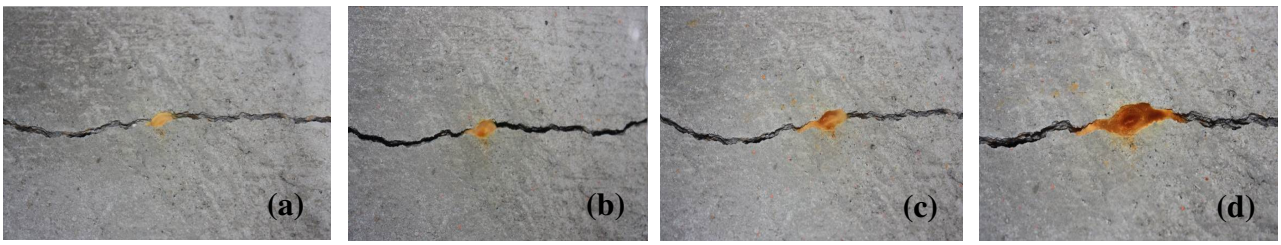

Figure 4: Corrosion product evolution in specimen Z11 (0.1-in-wide crack class) during exposure up to (a) 6 days (b) 20 days (c) 34 days (d) 52 days of continuous ponding to the 500 ppm chloride solution.

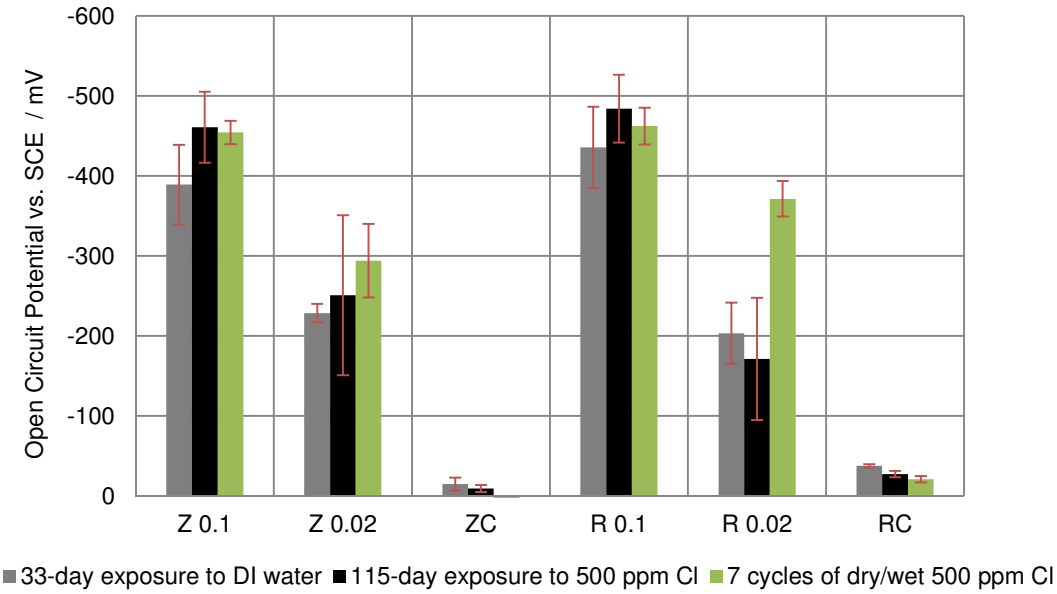

Figure 5: Average and range of open circuit potentials of duplicate specimens over the 3 exposure periods.

Potential mapping provided information indicating that the ongoing corrosion was indeed greater immediately below the cracks. Figure 6 (a) and (b) illustrate the potential maps for the specimens Z11 and R12, respectively, obtained during the cyclic exposure period to chloride-containing water. The maps indicate that all potentials are more negative than -350 mV versus SCE.

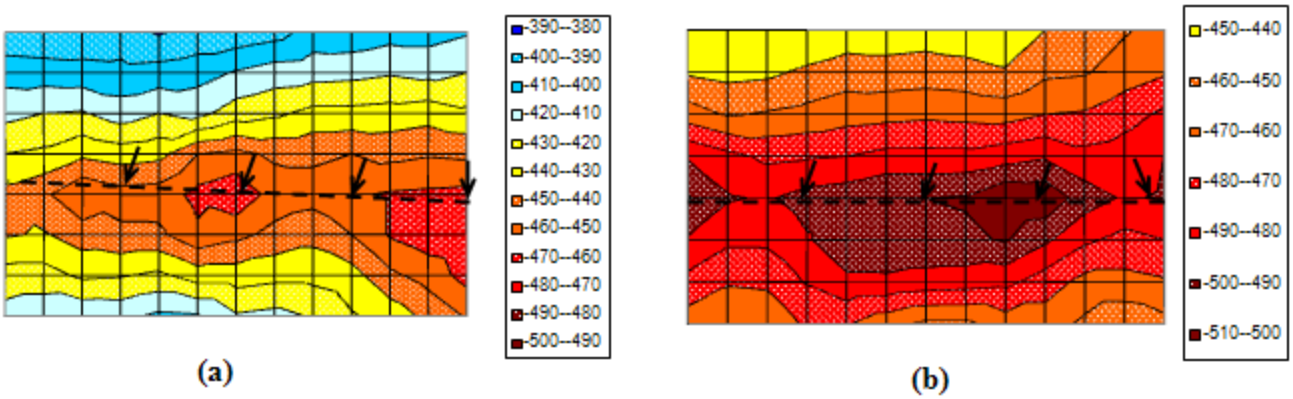

Figure 6: Potential mapping obtained during dry period of 5th dry/wet Cl$^-$ exposure cycle for 0.1 in (2.5 mm)-crack class specimens R12 (a) and Z11 (b). Broken lines: approximate location of crack; Arrows: steel wire intersection points. All potentials in mV vs. SCE.

The presence of extensive accumulated corrosion was confirmed on autopsy of specimens R12, R6, Z11 and Z1. Inspection of wire-crack intersections confirmed that all intersections exhibited corrosion damage, including those outside the ponding area, for 0.1-in-crack specimens of both RCP types. Figure 7 shows the corrosion damage at one of the crack-wire intersections of R12. The Z-type specimen in the 0.02-in-wide crack class also showed corrosion at all intersections, likely due to the presence of consolidation voids along circumferential wires. The R-type specimen in the 0.02-in-wide crack class showed corrosion only within the ponding area. The corrosion influence zones on each side of those intersections, measured in terms of wire diameter (D) on each side of the crack were on

average in the order of 2D, 1D, 15D and 30 D, for R12, R6, Z11 and Z1 respectively. Approximate measurements of actual radius loss over the influence zone were performed for Z11, R12 and R6 (uncertainty in diameter change was too great for Z1 given the spread of the corrosion influence zone) and converted to a total mass loss for each specimen . The results are plotted in Figure 10.

Figure 7: Corrosion influence zone at a wire-0.1 inch (2.5 mm) crack intersection of R12 after 246-day exposure to continuous and cyclic 500 ppm chloride environment

The EIS measurements provided quantitative information on the evolution of the corrosion rate as function of time and of the various exposure conditions. That information, after calibration as shown next, was used in formulating durability projection calculations.

Figure 8 (a and b) exemplifies the EIS behavior of cracked specimens having 0.02-in and 0.1-in class cracks, respectively, 65 days after continuous ponding exposure to 500 ppm-chloride. Figure 9 shows, as an example, the EIS behavior of specimen R4 after 65 days of continuous chloride ponding with the equivalent circuit fitting. The diagram shows that the low frequency end of the spectrum could be approximated relatively well by the analog circuit described earlier. The portion of the spectrum at frequencies higher than those sampled could be fitted by the circuit analog only with varying degrees of success. As a first approximation, data for only the frequency range from 0.01 to 0.001Hz were used for evaluation of Rp in all the tests addressed here for which the circuit analog fit was used.

The nominal polarization resistance for the data in Figure 8b is significantly smaller than those for Figure 8a indicating, per application of (3), a correspondingly higher nominal corrosion currents in the former, as expected. It is emphasized that given the uncertainties noted above, observations on corrosion behavior trends were based not only on the results of this particular pair of tests, but also on consideration of the results from multiple tests. The nominal value of Rp for specimen R6 (Figure 8a) was extremely large so the impedance diagram is dominated by the straight-line characteristic response of the CPE.[9] The corresponding nominal corrosion current per (3) is nil. The nominal value of Rp for Z1, Z13 and R3 (Figure 8a) was finite but still large and the fit line would show only very slight curvature.

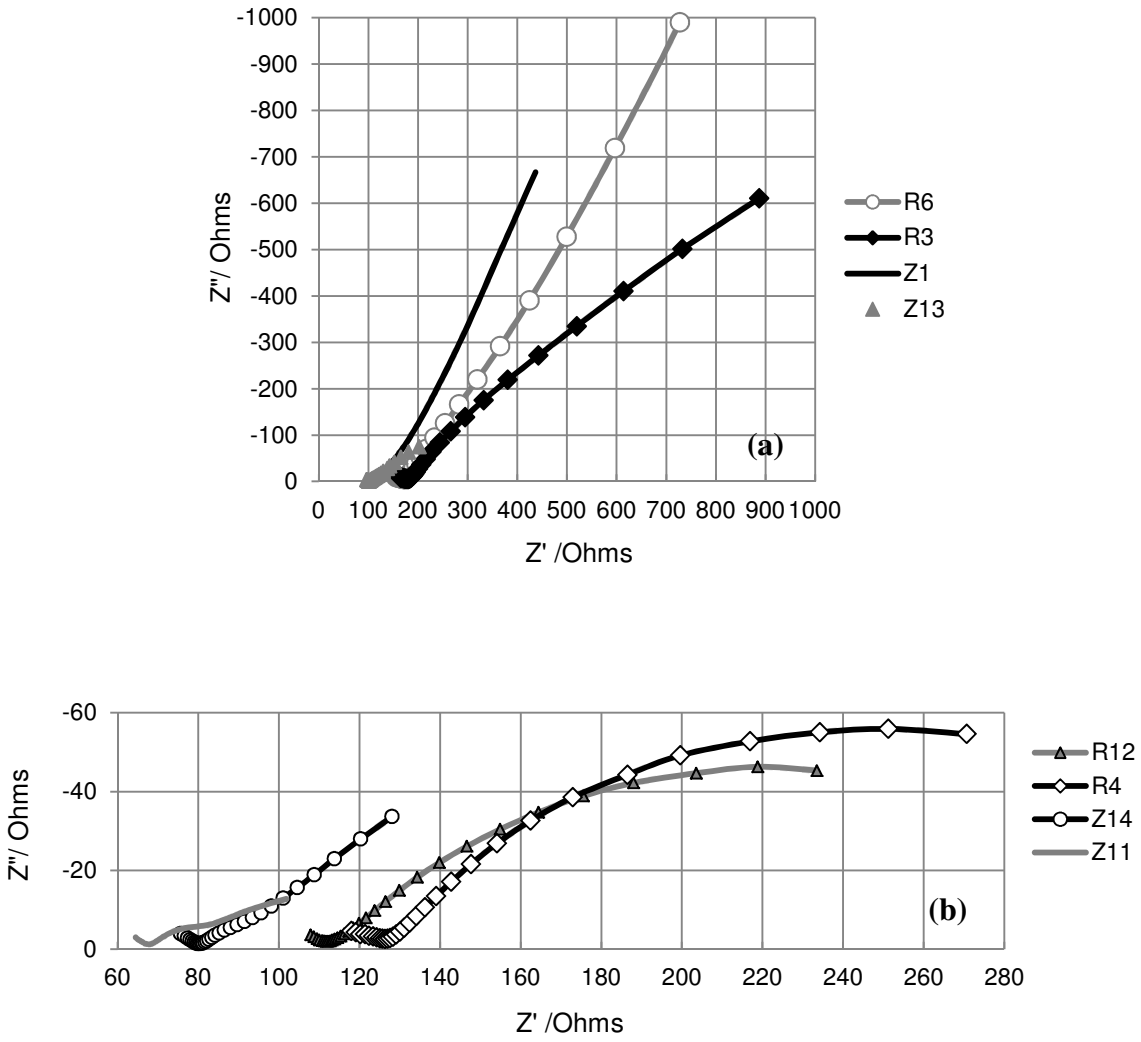

Figure 8: An example showing EIS spectra for Z- and R-type specimens in the (a) 0.02 in (0.5 mm) crack class and (b) 0.1 in (2.5 mm) crack class, after 65 days of continuous chloride exposure. Frequency range: 1mHz to 1000 Hz, 5 points per decade.

The nominal corrosion currents, (I), for each test date, were calculated from (3) and integrated (for each individual specimen) over the entire exposure period in order to obtain the corresponding total mass loss accumulating over time by means of the Faradaic conversion given by (4).

$$m = Q\, Aw_{Fe}\, F^{-1}\, v^{-1} \qquad (4)$$

Where, m is the amount of steel loss due to corrosion in g; Aw_{Fe} is the atomic weight of Fe (assumed on first approximation to make up the entire steel mass), 55.847 g/mole; F is Faraday's constant, 96,485 coul/equivalent; v is the effective valence corresponding to assuming that iron dissolves as divalent ions, 2; and Q is the total charge in coul such that for any given test point, (n), Q is approximated by (5) where, t is the length of exposure time in seconds.

$$Q_n = \sum_{n=1}^{m} (I_n - I_{n-1}) / t_n \qquad (5)$$

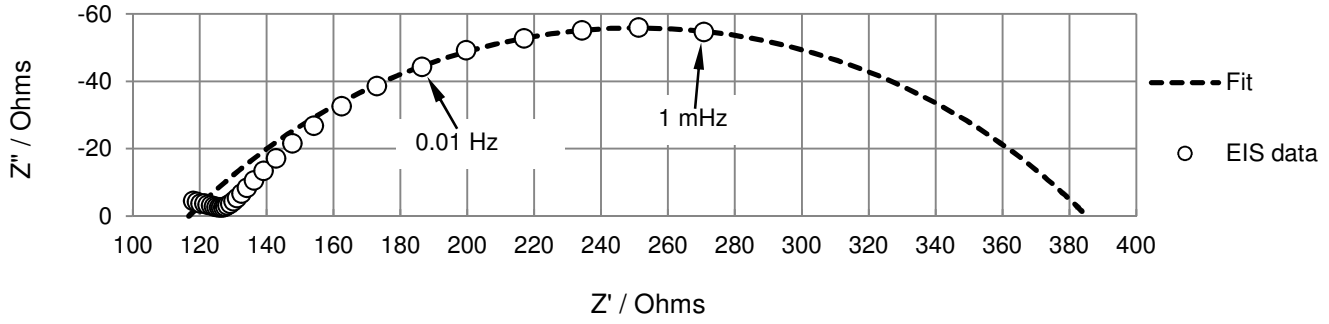

Figure 9: Equivalent circuit fitting of specimen R4 from Figure (8b). The broken line, extended to the zero frequency limit, is the fit obtained with the equivalent circuit when adjusting for the 1 mHz to 0.01 Hz data range only.

Application of (4) and (5) (assuming that corrosion during the dry portion of each cycle took place at about the same rate as during the wet portion) resulted in the graphs in Figure 10 that show the nominal accumulated mass loss for each individual specimen over the entire time span of all exposure conditions. Comparison of calculated mass loss based on EIS measurements with those from the destructive examination revealed that the former underestimated the corrosion currents. This finding was expected in the case of localized corrosion as reported in the literature, so a calibration procedure was in order.[12] The actual total mass loss for the autopsied specimens correspond to the production of up to 1.5 cm^3 of rust in the case of 0.1-in-crack owing to the expansive nature of steel corrosion products.[13] The effect of steel mass loss (in terms of equivalent radius loss) on corrosion-induced cracking will be discussed further in the durability projection section.

Table 3 summarizes the total mass loss values obtained from actual measurements and those calculated from EIS data. A calibration factor (Fc) was defined as Fc=Icorr/Iapp (or Fc=actual mass loss/apparent mass loss obtained from EIS); where Icorr is actual corrosion current and Iapp is apparent corrosion current calculated from EIS data. The values of calibration factor for the specimens examined showed close agreement with similar values reported in the literature based on the expected underestimation of corrosion rates from polarization measurements when small anodic regions are coupled with large cathodic regions.[12]

The nominal corrosion currents obtained from the EIS data for the Z- and R-type specimens were mulitplied accordingly by calibration factors of 1.25 and 3, respectively. Those corrected values are considered in the following discussion.

Figure 10 (b) shows the total mass loss (from either direct or calibrated indirect measurements) for all the specimens as a function of crack width-to-concrete cover ratio, separately for each type of RCP. The trend lines Figure 10 (b) suggest an increase in corrosion damage as the ratio of crack width to concrete cover increases. The steeper trend line for the Z-type may be attributed to more surface area of steel being exposed to corrosion than just that at the bottom of a crack, reflecting the presence of consolidation voids for that pipe type (Figure 2). This condition was confirmed by subsequent destructive examination.

The above concerns the corrosion current or mass loss integrated over the entire wire area of a specimen. The corrosion rate localized to the corrosion influence zone region only in each specimen is considered next. To that end Figure 11 shows, for each specimen, corrosion rates in the corrosion influence zones averaged over the entire exposure to all test environments. The R-type specimens exhibited higher corrosion rates due to corrosion localization (shorter influence zones) whereas the corrosion rates of the Z-type specimens were much smaller due to more distributed corrosion associated with the presence of consolidation voids along the wire.

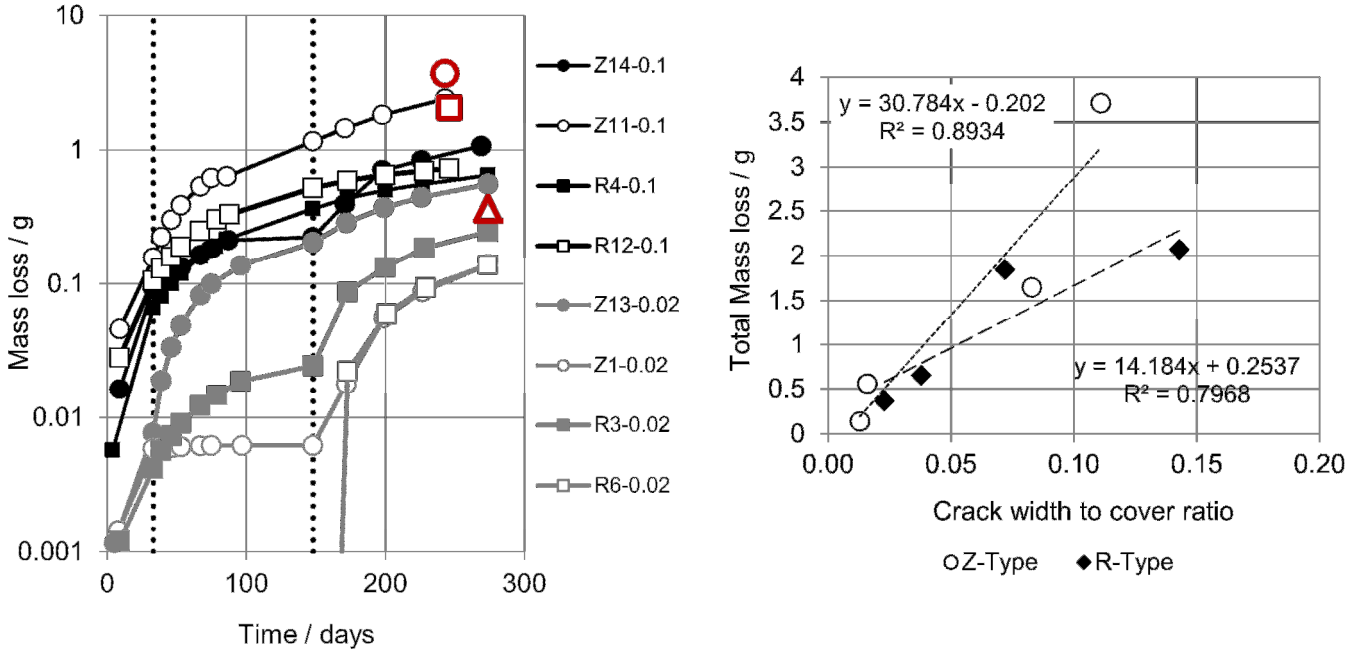

(a) (b)

Figure 10: (a) Black, grey and white symbols: nominal mass loss (uncorrected) based on EIS. Dotted lines at 33 and 148 days mark start of continuous and cyclic chloride exposure periods respectively. Red circle, square and triangle: mass loss for Z11, R12 and R6 respectively, from direct wire diameter loss, (b) Total mass loss (from either direct or calibrated indirect measurements) as a function of crack width-to-cover ratio for Z- and R-types.

Table 3
Actual and apparent mass loss values and the derived calibration factors (Fc)

Sp.#/Crack Width / inch (mm)	Time /days	Total Mass Loss /g		Fc= Icorr/Iapp	Anode/Cathode area ratio	Fc range from Sagüés et al[12]	
		Actual	Apparent from EIS			From	To
Z11/0.116 (2.94)	243	3.71	2.41	1.54	0.35	1.18	2
Z14/0.093 (2.36)	269	-	1.07	-	0.35	1.18	2
Z13/0.021 (0.53)	274	-	0.56	-	0.83	1.11	1.67
Z1/0.017 (0.43)	274	*	0.14	*	~1	1.05	1.54
R4/0.067 (1.70)	246	-	0.65	-	0.03	1.74	3.64
R12/0.106 (2.69)	246	2.07	0.73	2.84	0.03	1.74	3.64
R3/0.028 (0.71)	274	-	0.25	-	0.01	2.35	5
R6/0.018 (0.45)	274	0.37	0.14	2.64	0.01	2.35	5

* Actual wire radius loss was undetectable due to uniform corrosion indicating reasonable agreement with apparent EIS value.

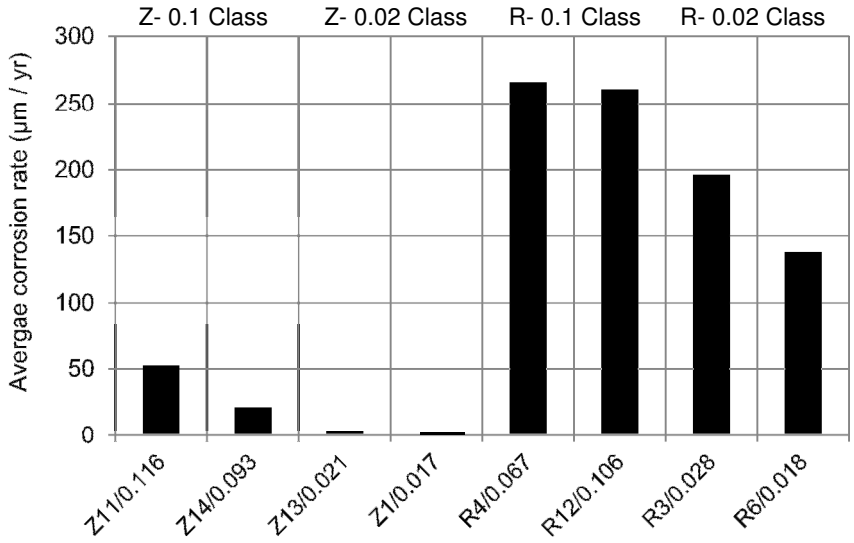

Figure 11: Corrosion rates in the corrosion influence zone (from either direct measurement or calibrated EIS data) averaged over the entire exposure of specimens to all test environments. The individual crack width in inch is shown for each specimen.

The time evolution of corrosion as the various exposure regimes took place can be appreciated (using again the corrosion current for the entire specimen) in the summary of results in Figure 12, compiled using EIS results calibrated as indicated above.

The results indicate trends in general agreement with those suggested by the OCP measurements and visual observations of rust: clear indications of ongoing corrosion for the wider crack specimens from both concrete mixtures, with greater severity occurring after the addition of chloride ions and even more so during cyclic ponding; some but significantly less corrosion present for the small crack width, and no measurable corrosion for the uncracked control specimens. The R-type specimens in the 0.02-in-wide crack class exhibited an increase in corrosion current by an order of magnitude under accelerated cyclic exposure which can also be seen from its OCP behavior. The intermittent exposure seems to have aggravated the corrosion process in the case of 0.02-in-crack class of both RCP types. The higher corrosion currents of Z-type specimens are associated with relatively large active corrosion zone leading to smaller corrosion rates as shown in Figure 11.

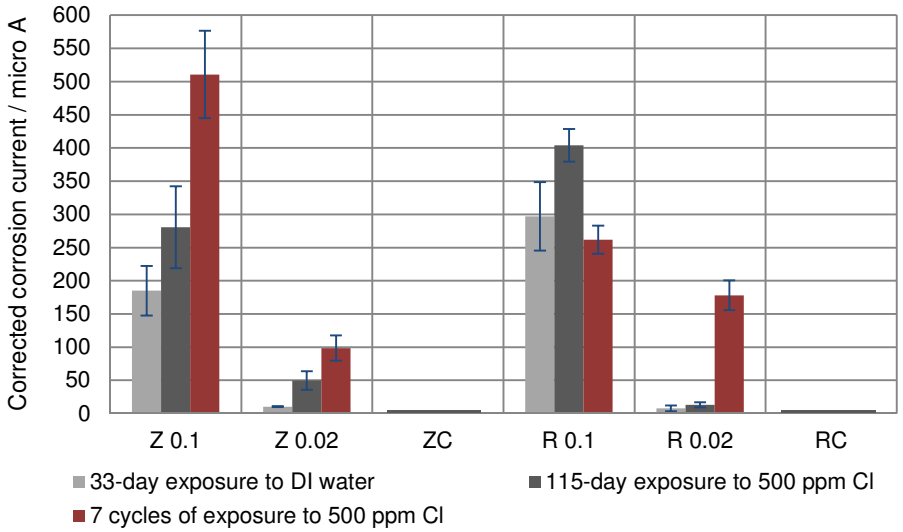

Figure 12: Corrosion currents (from calibrated EIS results) averaged over each exposure period

Exploratory Corrosion Projection and Overall Significance

The corrosion measurements described above provided an estimate of the amount of steel loss that was taking place as time progressed, for the various conditions evaluated. The physical effects of that corrosion, in particular the possible development of corrosion spalls depend not only on the total rate of metal loss but also on how localized that loss may be. The extent of corrosion localization determined by direct examination can be used as the basis for corrosion damage forecasts. A modeling approach is presented and implemented next to explore some possible consequences of corrosion in cracked concrete pipe. The model starts from the approach used in previous work that evaluated the corrosion progression in previously cracked concrete.[14] As shown in Figure 13, the active corrosion zone is identified to extend for a given corrosion influence distance (Li) on each side of the crack/wire intersections thus defining an active steel area for a given specimen size and wire placement density. The corrosion current (using as a basis the values estimated earlier on) is then divided by that total active area (A_i), resulting in a corrosion current density (i_A) that is converted into a corrosion rate. Calculations are then performed to assess durability in terms of projected time (t_f) to reach failure under an idealized failure scenario. Actual performance reduction involves complex situations beyond the chosen scenario. However, the quantitative estimates provided here serve to illustrate the time scales that may be involved in reaching pipe distress situations.

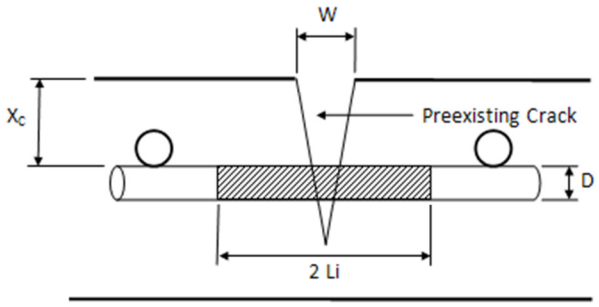

Figure 13: Conceptual crosswise intersection of reinforcing wire by preexisting crack

In these calculations the assumed failure event is spalling of the concrete cover due to the development of additional cracks created by expansive corrosion products in the corrosion influence zone.
For such calculations the corrosion rate value, together with the wire size diameter (D), concrete cover (X_c) and active zone size are used applying the empirical relationship developed by Torres (6), to obtain the time of service at which concrete spalls would develop.[15] That investigation addressed only sound concrete with no preexisting cracks, but its findings are used in the absence of comparable work with preexisting cracks. In that relationship the amount of corrosion needed to create expansive corrosion product leading to cracking and spalling is expressed in terms of a critical amount of metal radius loss in the wire, X_{crit}.

$$Xcrit\ /mm = 0.011\ (Xc / D)\ (1+Xc / 2Li)^2 \qquad (6)$$

The calculations were implemented to correspond to the specimens used in the experimental work described earlier. The total surface area of wire subject to corrosion is, $A_i = n_x \pi D 2L_i$, where n_x is the number of points where a crack intersects with a steel wire crosswise (n_x = 6 and 5 for the Z and R-types respectively) and D is the steel wire diameter, for which the nominal size ~ 3/16 in was adopted. The average concrete cover values used for the Z- and R-type specimens were 31 and 18 mm, respectively. The cases considered for the portions of steel wire influenced by corrosion, (Li) are 1D and 2D for the R-type RCP 0.02 and 0.1-in crack classes, and 30D and 15 D for the Z-type RCP 0.02

and 0.1-in crack classes respectively. The nominal projected time to corrosion induced cracking is thus estimated using (7).

$$t_f = (v\ F\ \rho\ X_{crit}) / (i_A\ Aw_{Fe}) \quad (7)$$

where ρ is the steel density, 7.8 g/cm^3

The cases treated in this projection assume exposure of RCP cracked specimens as though exposed to either continuous or cyclic chloride ponding. The average current for the duplicate specimens over each respective test condition from Figure 12 was used accordingly. The nominal projection results are summarized in Figure 14. The average of currents over wet periods was conservatively considered representative to the entire cyclic period.

As stated in the Introduction, this analysis is aimed to estimate the extent of corrosion damage that would occur, under the assumed scenario, in the absence of any mitigating AH effects. Some important additional qualifications apply. In the first place, as noted above, equation (6) was developed for cases where no preexisting cracking was present. In the present case, some stress relief may occur because of the loss of stiffness due to the preexisting crack, corrosion products growing into the preexisting crack instead of on the wire surface, especially for the wider cracks, and the formation of some of the corrosion products in liquid instead of solid form. Those factors would all tend to make the projections more conservative. The projections are also based on the simplifying assumption that the corrosion rates encountered in a short laboratory test period would remain the same over service times that may involve many decades. Again setting aside possible AH effects, corrosion rates could change with time, for example due to accumulation of corrosion products that may hinder the anodic reaction, resulting in further uncertainty in the projected damage.[16] The simplifying assumption was made in the absence of any corrosion rate prediction model for cracked reinforced concrete.[16] The labeling of the projections by Z- or R-type is made only to associate the projections with the variability of behavior that was encountered in the laboratory specimens, which is assumed to reflect to some extent the variability that may be encountered under normal production and use of pipe materials, and do not imply a particular advantage of one type of pipe manufacturer over the other. Finally, future work should focus on assessing the extent of corrosion-related distress of in-place RCP to ascertain the extent to which concrete deterioration mechanisms, such as the one hypothesized here, actually take place.

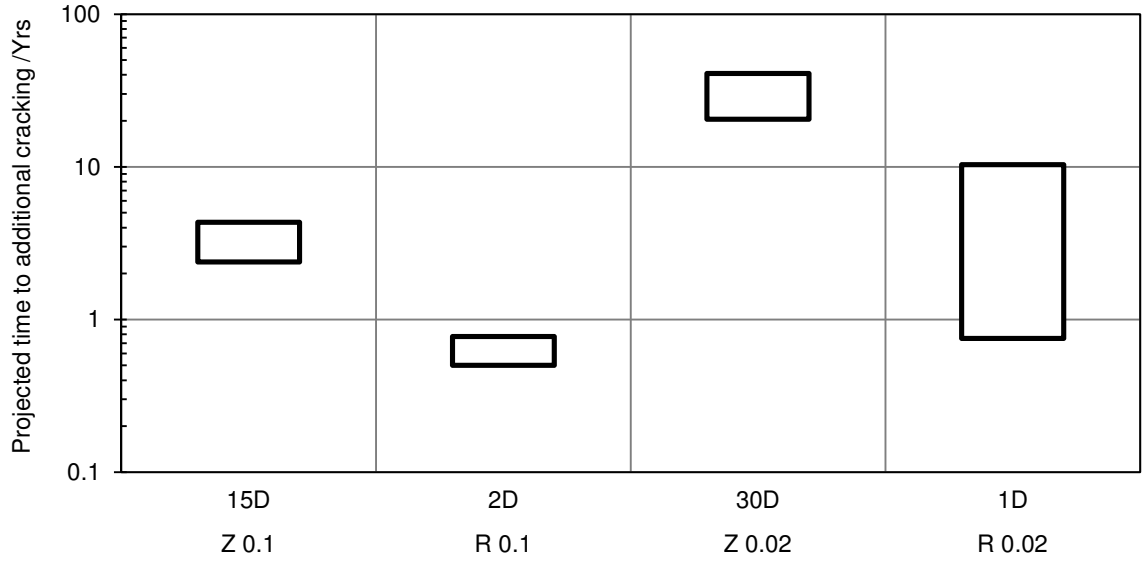

Figure 14: Nominal projected times to corrosion-induced concrete cover cracking. The extent of corrosion is indicated in terms of wire diameter on each side of the crack for the R- and Z-type specimens for the indicted crack class (in). The top and bottom ends of the floating bars correspond to continuous and cyclic exposure conditions, respectively.

With the above provisions in mind, projection values are considered only up to 100 years, which is in the order of the service life assigned to sound RCP by present design criteria (e.g. FDOT culvert life estimator), for service in mildly aggressive media such as the solution used here.[17] The estimated ranges of nominal time required for the formation of cracks, additional to the one already present at the beginning, are displayed in Figure 14 by floating bars for the 0.1 and 0.02-in-crack classes.

The projections for the 0.1-in-crack class cases yielded very short times to damage less than 5 years) under all test conditions. Even considering the conservative aspects of the projections noted earlier, the projections (as well as the direct observations of corrosion) support the concern that cracks this wide could have a significant detrimental effect on wire corrosion.

Under continuous exposure conditions, the 0.02-in-crack class cases exhibited much better prognosis ranging from 10 years (R-type) to ~ 80 years (Z-type). Given the effect of the consolidation voids in the Z-type material on corrosion current distribution as explained earlier, the greater length of corrosion influence seems to be the reason for the longer time to cracking.

Projections for the 0.02-in-cracks become comparatively pessimistic under accelerated cyclic exposure conditions approaching durations close to those for the continuous exposure for the 0.1-in crack cases. Furthermore, the laboratory cyclic regime with associated evaporative chloride ion concentration and frequent cycling may be an extreme not often encountered under field conditions. Hence and noting the general conservative character of these projections, this analysis suggests that the 0.02-in crack conditions tend to result in slow enough deterioration progression for a corrosion mitigating mechanism to take place in the interim.

CONCLUSIONS

1. Corrosion damage increased as the ratio of crack width-to-concrete cover thickness increased. Localized corrosion was observed at crack-wire intersections.

2. All RC pipe specimens having nominal 0.1 in (2.5 mm)-wide cracks of both concrete types (with and without fly ash) showed much higher corrosion currents than those having 0.02 in (0.5 mm)-wide cracks when exposed to both continuous and cyclic 500 ppm chloride environments.

3. RCP specimens having nominal 0.1 in (2.5 mm)-wide cracks exhibited relatively high corrosion currents and corrosion potentials even when exposed to de-ionized water.

4. RCP specimens having nominal 0.02 in (0.5 mm) -wide cracks, with a concrete cover thickness of about 1 inch (~25 mm), showed a better corrosion resistance when continuously exposed to 500 ppm chloride solution, whereas the accelerated cyclic exposure condition was found to have aggravated the corrosion process.

5. Simplified corrosion damage projections, based on corrosion-induced cracking failure scenario, yielded very short durability outcomes for 0.1 inch (2.5 mm)-wide crack cases. The analysis suggested that the 0.02 in (0.5 mm)crack conditions tend to result in slow enough deterioration progression for a greater chance of mitigating mechanisms to take place in the interim.

ACKNOWLEDGEMENTS

This work was supported by the Florida Department of Transportation. The opinions, findings, and conclusions expressed in this publication are those of the authors and not necessarily those of the State of Florida Department of Transportation. The authors appreciate the assistance of the University of South Florida structural laboratory and of the FDOT in providing and preparing the test specimens

REFERENCES

1. M. A. Pech-Canul and A. A. Sagüés, “Evaluation of Steel Reinforcement Corrosion in Concrete Drainage M.A. Culverts”, Corrosion/99, Paper No. 563 (Houston, TX: NACE 1999)

2. A. A. Sagüés, J. Peña, C. Cotrim, M Pech-Canul and I. Urdaneta, “Corrosion Resistance and Service Life of Drainage Culverts”, Final Report to Florida Dept. of Transportation (2001), Report No.WPI 0510756, Contract No. B-9898.

3. A. A. Sagüés, “Corrosion Measurement of Aluminum Alloys and Reinforced Concrete for Determination of Culvert Service Life”, Final Report to Florida Dept. of Transportation, Materials Office(1989), Report No. 99700-7324-010.

4. S. C. Kranc and A. A. Sagüés, A. A., “Computation of Corrosion Distribution Of Reinforcing Steel in Cracked Concrete”, in Proc. International Conference on Corrosion and Rehabilitation of Reinforced Concrete Structures, Orlando, FL, Dec. 7-11, 1998, CD ROM Publication No. FHWA-SA-99-014, Federal Highway Administration.

5. A. Neville (2002), "Autogenous Healing - a Concrete Miracle?", *Concrete International*, Vol. 24, Issue 11, p. 76.

6. E. R. Busba, A. A. Sagüés and G. Mullins, “Reinforced Concrete Pipe Cracks- Acceptance Criteria”, Final Report to Florida Dept. of Transportation (2011), Contract No. BDK84 977-06.

7. AASHTO (American Association of State Highway and Transportation Officials) (2006), LRFD Bridge Construction Specification, Section 27, Concrete Culverts, Clause (27.4.1), Washington DC.

8. ASTM (2011) [(A)], C76 – 11 “Standard Specification for Reinforced Concrete Culvert, Storm Drain, and Sewer Pipe”, American Society for Testing and Materials, Philadelphia, PA.

9. A. A. Sagüés, “Corrosion Measurement Techniques for Steel in Concrete”, Paper No. 353, Corrosion/93, NACE International, (1993), Houston, TX.

10. C. Andrade and J. A. Gonzalez, “ Quantitative measurements of corrosion rate of reinforcing steels embedded in concrete using polarization resistance measurements”, *Werkstoffe und Korrosion,* (1978), Vol. 29, p.515.

11. ASTM (2009), C876 – 09 “Standard Test Method for Half-Cell Potentials of Uncoated Reinforcing Steel in Concrete”, American Society for Testing and Materials, Philadelphia, PA.

12. A. A. Sagüés and S.C. Kranc, “Computer Modeling of Effect of Corrosion macrocells on Measurement of Corrosion rate of Reinforcing Steel in Concrete”, techniques to assess the corrosion activity of steel reinforced concrete structures, ASTM STP 1276, Neal S. Berke, Edward Escalante, Charles Nmai and david Whiting, Eds., ASTM,1996.

13. T. D. Marcotte, “Characterization of Chloride-Induced Corrosion Products that Form in Steel-Reinforced Cementitious Materials, PhD Thesis in Mechanical Engineering., (Waterloo, Canada: University of Waterloo 2001)

[(A)] ASTM International, 100 Barr Harbor Dr., West Conshohocken, PA 19428-2959.

14. K. Lau, A. A. Sagüés and R. Powers, “Effect of Concrete Environment on the Corrosion Performance of Epoxy-Coated Reinforcing Steel”, *Corrosion* 2010, Vol. 66, p. 065002.

15. A. Torres-Acosta and A. A. Sagüés, “Concrete Cracking by Localized Steel Corrosion - Geometric Effects”, *ACI Materials Journal 2004*, Vol. 101, p.501.

16. M. Otieno, H Beushausen and M. Alexander, “Prediction of Corrosion Rate in RC Structures- A critical review”, *Modelling of Corroding Concrete Structures*, RILEM Book series 5, (2011), DOI 10.1007/978-94-007-0677-4-2.

17. Florida Department of Transportation, “FDOT Drainage Handbook, Optional Pipe Materials”, 2010 (Tallahassee, FL: 10/20/2010). http://www.dot.state.fl.us/rddesign/dr/Manualsandhandbooks.shtm